

Measurement of boundary layer velocity profiles by ultrasonic tomography for the prediction of flow separation

AIAA flow control conference San Francisco 2006

Philip P. Geoghegan* and William J. Crowther†

University of Manchester, M30 7RU, England

Norman Wood‡

University of Manchester

A method for predicting flow separation is needed for the industrial application of some types of flow control. This should be on-board the aircraft and must be robust in order to achieve certification. Conventional non-intrusive sensors are unable to measure turbulent boundary layer(TBL) parameters that would be useful for the prediction of separation. Lab based techniques such as PIV and hot-wire are unsuitable for production aircraft. This paper introduces a novel method to measure TBL parameters using ultrasound.

Most ultrasonic flow measurement techniques require seeding of the flow or opposing transducers. The method introduced here employs a transmitter with a number of receivers located on the same wall. The time of flight between a transmitter and a downstream receiver is a function of their separation. However, the relationship is not linear, as convection of sound occurs and the propagation paths are curved. It will be shown that this time of flight can be used to determine the TBL profile.

The system was modelled using the method of ray acoustics. This method can be derived by assuming that the sound has an infinitely small wavelength. This is appropriate for simple modelling of ultrasound, capturing refraction effects but neglecting diffraction and absorption. Experimental results indicate that the modelling was appropriate.

The work presented here introduces a new method for performing non-intrusive measurements of a TBL. Knowing the state of a TBL will assist in the prediction of flow separation. Accurate separation prediction may prove to be a valuable tool in order to integrate flow control systems into production aircraft.

Nomenclature

A	Function representing boundary layer model	
c	Speed of sound	
c_{ref}	Reference speed of sound	
c_{exp}	Speed of sound during experiment	
E	Error function for difference between experiment and model	
M	Mach number	
\mathbf{n}	Vector representing normal to wavefronts for ray simulation	$\frac{U_0}{c}$
p	Mean velocity of the acoustic pulse in tunnel frame of ref.	$[n_1, n_2, n_3]$
p_e	Mean velocity of the acoustic pulse, predicted using ray model	$\frac{\epsilon_i}{t_{fc}(\epsilon_i)}$
R	Function representing ray model	
t_f	time of flight for acoustic signal	

*PhD Student, Aerospace Engineering, Goldstein Laboratory, Liverpool Road, Eccles, Manchester

†Senior Lecturer

‡Professor of Aerospace Engineering, SMAIAA

t_{fc}	Temperature corrected time of flight	
T_{ts}	Wind tunnel static temperature in working section	
\mathbf{U}	Fluid mean velocity on aerodynamic scale	$[U_1, U_2, U_3]$
U_0	Fluid mean velocity in x_1 direction outside boundary layer	
U_1^+	Non-dimensional U_1	$\frac{U_1}{u^*}$
u^*	Friction velocity	$\sqrt{\frac{\tau_w}{\rho}}$
\mathbf{v}	Fluid velocity perturbation representing aerodynamic turbulence	$[v_1, v_2, v_3]$
ν	Fluid kinematic viscosity	
\mathbf{w}	Fluid velocity perturbation for acoustic waves	$[w_1, w_2, w_3]$
\mathbf{x}	Position vector in Cartesian space	$[x_1, x_2, x_3]$
x_2^+	Non-dimensional x_2	$\frac{u^* x_2}{\nu}$
α_0	Initial condition for angle of ray	$Tan^{-1} \frac{n_2}{n_1}$
δ	Boundary layer thickness, $U_1 = 0.99U_0$	
δ_t	Thickness of viscous sublayer region of boundary layer	
δ_t^+	Non-dimensional δ_t	$\frac{u^* \delta_t}{\nu}$
ϵ	Separation of microphone and spark in x_1 direction	
ϵ_{min}	Minimum separation of microphone and spark used in experiment	
ϵ_{max}	Maximum separation of microphone and spark used in experiment	
κ	Constant in boundary layer model	
λ	Acoustic wavelength	
Π	Constant in boundary layer model	
ρ	Fluid density	
τ_w	Boundary layer wall shear stress	$\left(\frac{\partial U_1}{\partial x_2}\right)_{x_2=0}$

I. Introduction

The need to predict when a flow will separate occurs for a variety of industrial problems. The primary focus of this work is that it considers how to implement an on-board flow separation prediction capability for aircraft. One example of where this capability would be useful is in partnership with active flow control technologies. As a method for delaying flow separation an AFC system would need to know where and when separation was most likely to occur in order to prevent it. For simple geometries, it could be noted that separation occurs at a repeatable location at a given incidence. However, once geometries become sufficiently complex, subject to flexibility, icing and unsteady conditions, the prediction of flow separation from prior experience becomes difficult. This is where an on-board flow sensing system would be necessary. For a system implemented on a real aircraft, sensors are only likely to be permitted on the surface of the body. Protuberances into the flow would increase drag, especially if measurements at a large number of locations was desired. The problem that this work will address is that of predicting flow separation on a production aircraft by only placing sensing devices on the surface of the body. It is worthwhile briefly clarifying the difference between the detection of turbulent flow separation and its prediction.

SEPARATION DETECTION The detection of flow separation is possible using a number of techniques.¹ Measuring surface shear stress distributions is the most direct. However, measuring shear stress accurately is not an easy task, especially in hostile environments. The less direct method of looking at the spectral content of surface pressure may be more practical.² Either way, it seems possible for an aircraft mounted system to detect flow separation using conventional sensors.

PREDICTION OF SEPARATION Often the prediction of flow separation has been studied to develop good models for aerodynamic design. These methods usually predict an entire flow field for a given geometry. In contrast, the real time prediction of separation of aircraft flows is quite different, with geometry or boundary conditions possibly unknown. This is a little similar to inverse aerofoil design. The separation prediction may be accomplished as follows. By performing measurements on a body and identifying the most likely aerodynamic flow, it can be determined by some metric whether the flow is close to separation. The identification method may be statistical in nature or physically based. However, it is felt that in general

the prediction will be better if the measurements taken on the body are physically relevant to separation. If Turbulent Boundary Layer(TBL) parameters could be measured then applying integral boundary layer models would be ideal for predicting potential separation locations.

Conventional non-intrusive sensors are unable to measure TBL parameters such as shape factor and boundary layer thickness. These parameters would be useful for the identification of the flow-field, necessary for the prediction of separation. This is the motivation for the work presented here. Achieving a measurement of time averaged TBL parameters would be very useful. Most lab based techniques for fluid dynamic measurement would not be suitable for application to real aircraft. For instance PIV requires seeding of the flow and hot-wires are intrusive. Therefore a number of alternative methods were looked at. Most of these methods were different forms of tomography.

A. Tomographic techniques

For the non-intrusive determination of boundary layer parameters, a number of mechanisms were considered. Most of these involved the input of energy of a particular form, measuring what happens to the energy and comparing the result to a model of what normally happens in a given boundary layer.

The form of energy input could be thermal, optical, acoustic or some other. Optical methods generally need seeding particles or optics on both sides of the flow, both impossible for this problem. Thermal energy input has been used in the past for the determination of shear stress,³ a useful boundary layer parameter. However it seems unlikely that many other parameters could be identified using these techniques. Acoustics seems promising for providing a mechanism for simple boundary layer measurements. In particular, due to the small spatial extent of boundary layers, ultrasound would be the most practical.

The study of flows using ultrasound has been looked at by many authors. Doppler shift velocimetry⁴ has been accomplished in clear water and for atmospheric studies, but the required signal to noise ratio for the transducers was unrealistic for this application. Speckle imaging velocimetry⁵ is an interesting method, but requires seeding of the flow. Line of sight measurements⁶ are possible without seeding, but require one external sensor which is not possible for this problem.

The method proposed in this paper is similar in many ways to the research carried out on atmospheric boundary layers.⁷ If a short burst of ultrasound is emitted at a given location on the wall, under a turbulent boundary layer, the boundary layer itself will affect how the sound propagates. The sound propagation solution is non-trivial, involving scattering, dissipation and refraction due to velocity gradients. Over short transmission distances the scattering and dissipation effects are small. The effect of velocity gradients on sound propagation will be utilised to measure TBL profiles.

Velocity gradients cause the direction of sound propagation to change. This is shown schematically in Fig. 1 for a linear velocity gradient. When the sound starts propagating downstream and away from the wall, the sound follows a curved path back towards the wall. If the sound had been propagating upstream then it would have followed a path that curved away from the wall.

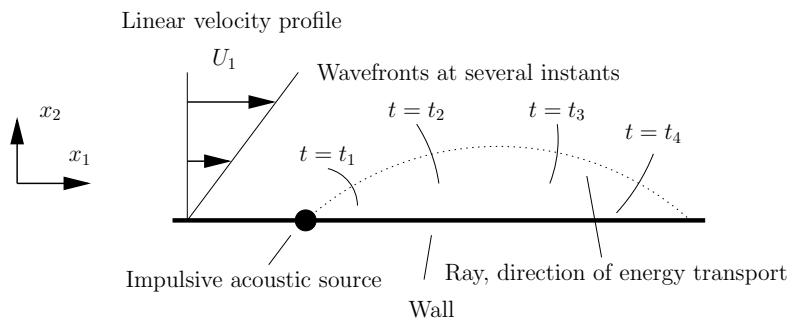


Figure 1. Schematic of downstream pulse propagation in a linear velocity gradient

The downstream propagation of sound in a boundary layer will be used to perform measurements of the flow. The arrival time of a pulse to different distances downstream will be the key aspect. The use of acoustics for fluid dynamic measurement requires a good understanding of the underlying physics of sound propagation. The next section will give the theoretical basis for sound propagating in a moving fluid.

An experimental verification of the theory will then be performed. Finally, this will lead to a method for determining parameters such as boundary layer thickness from experimental acoustic measurements.

II. Theoretical model

The subject of wave propagation in an unsteady moving media is complex. Numerous methods for modelling wave propagation are available in the literature.⁸ Two of particular interest are the ray model and the solution of the Linearised Euler Equations (LEE). Initially both methods were used for simulations. However, the computational efficiency of the ray model lead to its use for the majority of the work. Therefore only the ray model will be presented in the following section.

A. Ray model

A simple method for understanding the propagation of sound in a velocity field is by using a ray model. A ray is a curve that remains normal to the wavefronts, as indicated in Fig. 1. By modelling just the rays it is no longer necessary to model the entire wave field. Single rays can be calculated independently.

The ray model is based upon the assumption that the wavelength of the sound is small compared to the length scales present in the velocity field. For the experimental work presented later, the ratio of $\frac{\lambda}{\delta}$ was around 20, so was reasonably large. The assumption of small wavelength (geometric acoustics) can be applied to an unsteady moving media. This was first studied by Engleke.⁹ More recently, Pierce¹⁰ derived the same equations, but started with the fundamental equations of fluid dynamics. These are presented in Eq. 1 and Eq. 2. The vector \mathbf{x} represents the position of the ray at a given instant. The vector \mathbf{n} is used to represent the wave normal. The initial conditions that are required to solve the equations are the starting position, \mathbf{x}_0 and starting direction, \mathbf{n}_0 . The velocity and sound speed fields, $\mathbf{U}(\mathbf{x}), \mathbf{v}(\mathbf{x}, t), c(\mathbf{x}, t)$ are prescribed in advance of obtaining a solution for the rays.

$$\frac{d\mathbf{x}}{dt} = c\mathbf{n} + (\mathbf{U} + \mathbf{v}) \quad (1)$$

$$\frac{d\mathbf{n}}{dt} = -[\nabla - \mathbf{n}(\mathbf{n} \cdot \nabla)]c - \sum_k n_k [\nabla - \mathbf{n}(\mathbf{n} \cdot \nabla)](U_k + v_k) \quad (2)$$

For the simulations performed here, the equations above were somewhat simplified. It was assumed that the turbulent velocity, \mathbf{v} , was zero, that the solution was two dimensional in $[x_1, x_2]$ and that the speed of sound was constant throughout the boundary layer. The equations given in Eq. 3 and Eq. 4 were used for all ray simulations presented in this paper. The solution method was a fourth order Runge-Kutta integration with variable step-size.

$$\frac{d\mathbf{x}}{dt} = c\mathbf{n} + \mathbf{U} \quad (3)$$

$$\frac{d\mathbf{n}}{dt} = - \sum_k n_k [\nabla - \mathbf{n}(\mathbf{n} \cdot \nabla)]U_k \quad (4)$$

III. Experimental method

The ray model utilised several simplifying assumptions. The following experiment was designed to test that these were reasonable. In addition, the experiment would also verify that it is possible to construct a system with real actuators and sensors, that produces an adequate signal to noise ratio.

A. Description of experiment

A schematic of the experiment is shown in Fig. 2. The ultrasonic transmitter was a 70J spark source.¹¹ The electrical circuit and electrode arrangement define the sparks' acoustic properties. The configuration used by Wyber¹² was replicated. This resulted in a short ultrasonic pulse which was broadband and centered around $60kHz$. Crucially for this experiment, spark generated acoustic pulses begin with a fast rise to full amplitude. This allows the arrival time of the start of the pulse to be well defined. The spark source behaves

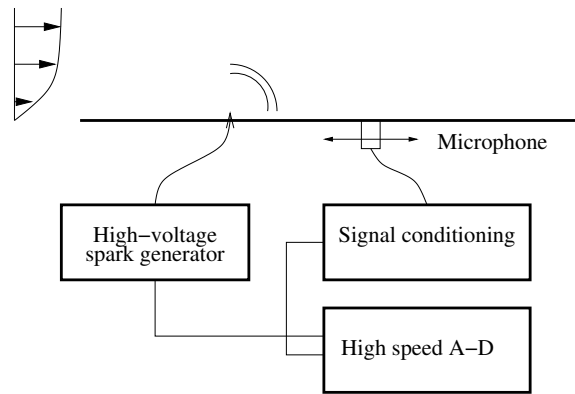


Figure 2. Data acquisition setup

like a point source in acoustic terms when the spark is short compared to the sound wavelength. In this case, the spark length was 1mm and the wavelength of the pulse around 3mm so the directivity of the source may not be perfectly spherical.

The ultrasound receiver was a Bruel & Kjaer type 4135 microphone. This has a bandwidth that extends to around 100kHz . The spark current, spark voltage and received signal were recorded at 5Mps in 12bit voltage resolution. The high sampling rate was necessary to give sufficient resolution for temporal information such as the time of flight.

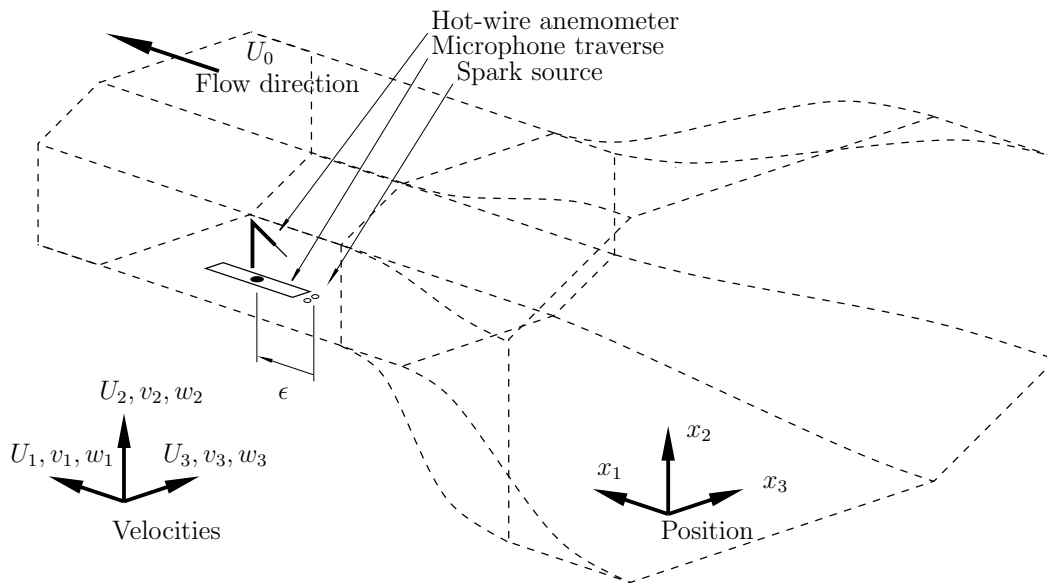


Figure 3. Experimental setup

A microphone traverse was fabricated to move the position of the microphone relative to the spark. In order to maintain a flat wall for the aerodynamic boundary layer, an arrangement of sliding panels was used. These were moved using a stepper motor over a travel of 400mm . The various contributions to error in the position of the microphone were assessed, resulting in an estimate of $\pm 0.3\text{mm}$. Similarly, an automatic hot-wire traverse was available for measuring the true boundary layer parameters.

The wind tunnel used was the Avro tunnel situated at the Goldstein Laboratory in Manchester. This large closed return type tunnel had a working section of $2.7 \times 2.1\text{m}$. The microphone traverse, spark source and hot-wire traverse were located in the center of a floor panel in the working section as shown in Fig. 3. The boundary layer on the floor had developed through the convergent section of the tunnel and over

approximately 3m of flat floor panel before arriving at the location of the experiment.

The experimental setup was fully computer automated, allowing good control of experimental conditions. However, at the facility used, the tunnel temperature tended to rise continuously throughout testing. Therefore the tunnel temperature was monitored and recorded so that corrections could be introduced later. The testing procedure was as given in the next section.

B. Experimental procedure

1. The hot wire was calibrated in the free stream and then used to measure the boundary layer profile. A second calibration was performed after taking measurements to assess calibration error.
2. With the tunnel turned off, a complete set of measurements were performed using the spark and microphone. For each spacing of spark and microphone the results from the propagation of ten spark events were recorded. This test, with $U_0 = 0ms^{-1}$, was a null run and was used for assessing the error sources for the spark-microphone part of the experiment.
3. Finally, the tunnel was run at the velocity used earlier for hot-wire results, 1, and the spark results recorded in the same manner as the null test.

The measurement of hot-wire results, null experiment and spark experiment (steps 1-3) were repeated for the three tunnel velocities $U_0 = 40, 50, 60ms^{-1}$.

C. Data processing procedure

The measurements of microphone voltage as a function of time were converted to a single valued time of flight. This was performed as follows. The mean of the microphone signal was removed and the amplitude normalised on the peak-peak amplitude of the pulse. Ten microphone time series were averaged removing the relatively low frequency and low amplitude pressure fluctuations due to turbulence. A threshold of 0.5 was used to determine the arrival time of the pulse. Subtracting the time offset of the spark event gives the time of flight, t_f . This was repeated for all separations, ϵ , between spark and microphone.

The wind tunnel static temperature, T_{ts} , was not constant throughout the experiment. It was recorded so that it could be used to correct the measurements of time of flight. When the atmospheric pressure is close to sea level ISA, Eq. 5 can be used to obtain a good estimate of the speed of sound. As this was the case, the experimental speed of sound, c_{exp} , was calculated for all the tunnel temperature measurements.

$$c_{exp} = 20.05\sqrt{T_{ts} + 273.15} \quad (5)$$

In order to be able to compare experimental results taken at different tunnel temperatures, the time of flight, $t_f(\epsilon_i)$, was corrected to a reference speed. Here the reference speed of $c_{ref} = 340.0ms^{-1}$ was used. The relation in Eq. 6 was used to correct all the time of flight results shown in this paper.

$$t_{fc}(\epsilon_i) = \left(\frac{1}{t_f(\epsilon_i)} - \frac{c_{exp}}{\epsilon_i} + \frac{c_{ref}}{\epsilon_i} \right)^{-1} \quad (6)$$

A good way of representing the time of flight is by defining the mean pulse velocity as the separation distance divided by the time of flight, as given in Eq. 7.

$$p(\epsilon_i) = \frac{\epsilon_i}{t_{fc}(\epsilon_i)} \quad (7)$$

When the medium is stationary, p should equal the speed of sound in the medium for all separations, ϵ . The variation of p with microphone-source spacing ϵ for propagation in a moving media will be discussed in subsequent sections.

IV. Results

The results from both the numerical simulations and the experimental work will be compared in this section. Then the experimental results will be used to perform a measurement of the boundary layer state.

A. Numerical results

Results from integrating the ray model presented in §II.A, are shown in Fig. 4. The rays are sent in a downstream direction, and curve towards the wall as expected. The initial angle of the ray determines whether the ray curves back to the wall or passes through the boundary layer (as the $\alpha_0 = 28^\circ$ case does). A ray that impinges upon the wall may be expected to be reflected from the wall, leading to multi-path solutions. Important information can be realised from looking at the time of flight. At a particular location downstream of the transmitter, the first ray to arrive at that location is always the direct one, not one which has reflected off the wall (for boundary layer velocity profiles without inflections). Therefore the arrival time of the ray can be measured without interference from multi-path solutions.

The fact that the rays reach a maximum height in the boundary layer during their propagation is useful. It results in the fact that the information contained in the time of flight of a particular ray can only be function of the flow below this maximum height.

Consider two rays, the first impinges upon the wall close to the transmitter and reaches a small maximum height in the boundary layer. Its time of flight is a function of the flow near the wall only. A second ray which impinges the wall slightly further downstream will have travelled to a slightly higher maximum. The information in the time of flight of the second ray will be a function of the same flow as the first ray and the flow between the maximums of the first and second rays. This gives an indication that a knowledge of the time of flight to several different distances along the wall may enable an estimation of the boundary layer profile.

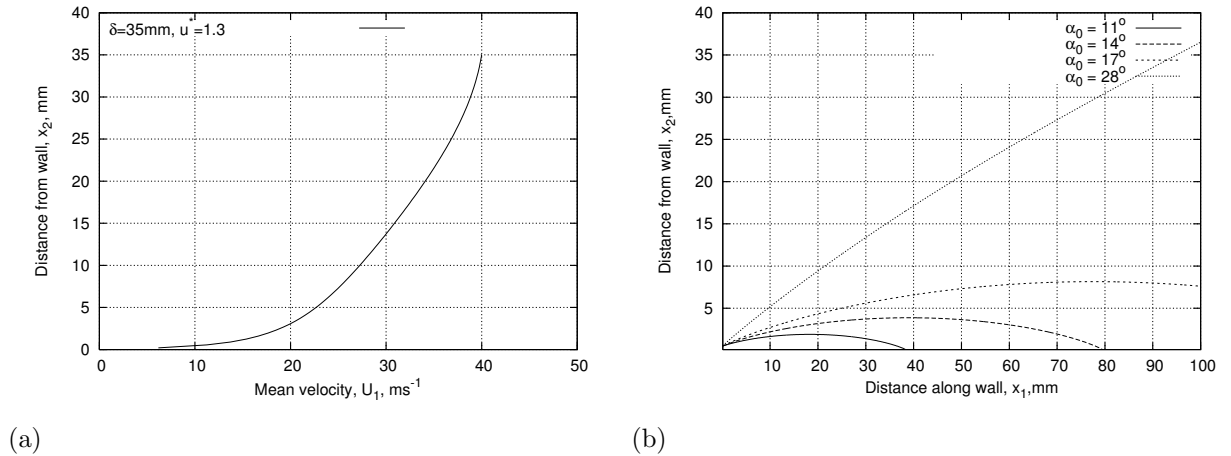


Figure 4. Sample solution of ray equations: (a) Example boundary layer profile using log velocity defect law: (b) Corresponding numerical results for ray paths with several initial conditions

The following numerical work was performed in order to show how the time of flight over different separations, ϵ , is affected by the boundary layer. Three examples of boundary layer profiles were computed, as shown in Fig. 5(a). These were then used as the flow conditions for the ray model. A number of rays with different initial conditions were computed in each boundary layer. The results were processed to extract the time of flight to different distances along the wall. In such a way, theoretical curves could be calculated for the mean pulse velocity as a function of distance before the ray impinges the wall, $p_e(\epsilon)$, Eq. 7. These curves are shown in Fig. 5(b).

When a boundary layer is present, the mean pulse velocity is bounded by two values. The mean pulse velocity cannot be slower than the speed of sound in the medium, c . It can be faster by convection up to the limit of the speed of sound plus the free-stream velocity, $U_0 + c$. These limits are shown in Fig. 5(b). As expected, all the theoretical curves lie between these two extremes.

The results shown in Fig. 5 highlight several features. The effect of halving the boundary layer thickness can be observed by comparing cases 1 and 2. Halving TBL thickness results in a $p_e(\epsilon)$ curve which is a similar shape, but seems scaled by a factor of a half in ϵ . Changing u^* effectively changes the shape factor of the boundary layer profile, as in cases 1 and 3. This results in a $p_e(\epsilon)$ curve that has a different shape. General conclusions about the shape of the $p_e(\epsilon)$ curves are difficult to make due to the non-linear nature of the ray algorithm.

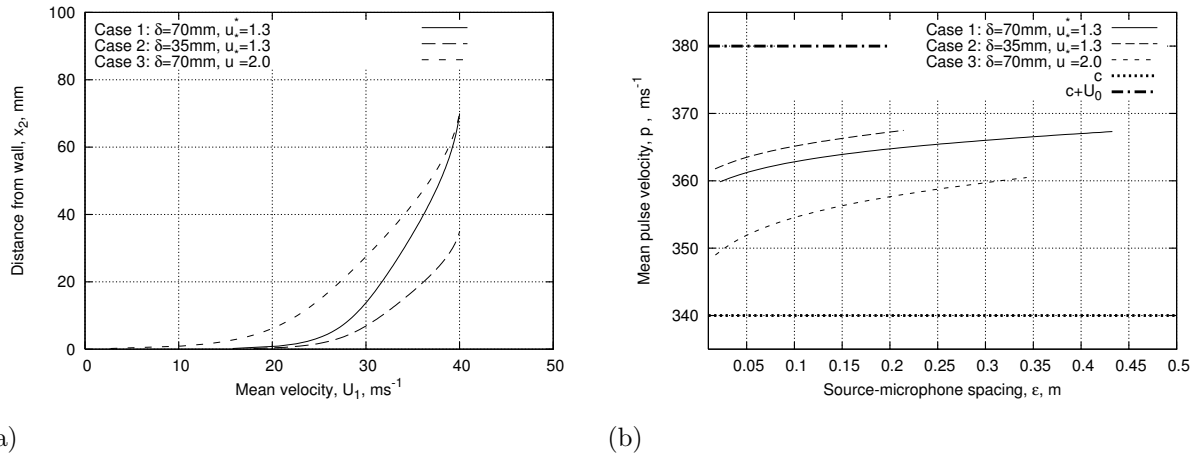


Figure 5. Effect of different boundary layer profiles on the shape of the mean propagation velocity curve, p : (a) Example boundary layer profiles using log velocity defect law: (b) Corresponding numerical results for mean propagation velocity

B. Experimental results

The results given in the next section are concerned with assessing the performance of the combination of acoustic source and microphone. Subsequently, the results for acoustic propagation and a comparison to the ray model will be given.

1. Characteristics of the transducers

A number of examples of the acoustic pulse recorded are shown in Fig. 6. The measured microphone signal was normalised on the peak-peak voltage of the pulse and offset in time to align all the pulses for plotting. The pulse remains a relatively similar shape over the distances involved in this experiment, although a loss in coherence is evident. This loss in coherence would be expected as a result of interference of waves travelling in different paths. After the initial cycles it can be seen that there is a continuing oscillation at around $60kHz$. This was thought to be some form of resonance and the frequency is not far from the microphone resonance of $100kHz$. However, the experiment is only concerned with the arrival time of the pulse so only the shape of the initial rising edge is of significance.

The amplitude of the pulse is of significance and is shown in Fig. 7 as a function of propagation distance. Here, the maximum peak-peak microphone voltage is used to represent the pulse amplitude. If the spark length was small compared to the wavelength of the pulse, one would expect it to behave like an idealised point source. In a stationary medium, ($U_0 = 0ms^{-1}$), this should produce spherical waves. The graph shows a line of slope ϵ^{-2} which applies to spherical spreading. However, the measured data has a slope of ϵ^{-1} which would correspond to an ideal cylindrical source in a stationary medium. It is surprising that the data had this slope and could be the result of a number of causes. The presence of the wall, vibration of the electrodes (rods end to end, aligned in the x_3 direction) and directivity of the source are all complicating factors.

Of particular interest in Fig. 7 is the behaviour of the amplitude of the pulse when there is a boundary layer present. Unlike propagation upstream, propagation downstream causes the sound rays to converge, resulting in a significantly reduced drop in amplitude over distance. This is an advantage in practical terms since it permits smaller amplitude pulses to be used before the signal to noise ratio of a given microphone is exceeded.

2. Acoustic propagation results

A useful test that the system was working correctly was the null test, with the tunnel stopped and $U_0 = 0ms^{-1}$. The results for mean pulse velocity are shown in Fig. 8. As expected the results are close to the reference speed of sound in the medium for all spacings. This confirms that both the experimental system is performing as expected and the temperature correction method is appropriate. Of particular interest are

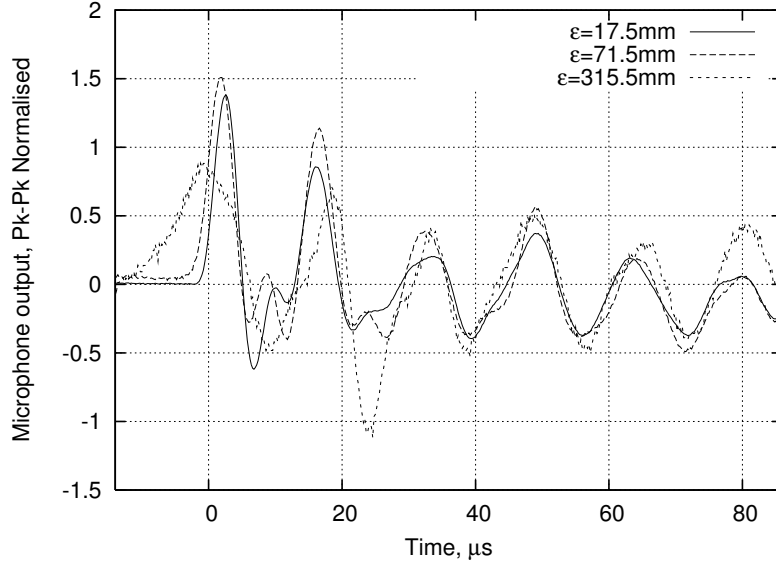


Figure 6. Time series of microphone response to ultrasonic pulse at several source-microphone spacings, with boundary layer flow, $U_0 = 40ms^{-1}$

the error-bars for p which were computed based upon the uncertainty in the separation, ϵ . This error source becomes significant as the spacing becomes small.

Calculation of the pulse velocity from microphone results with the $40ms^{-1}$ boundary layer are shown in Fig. 9. A numerical simulation using the ray model with the experimental boundary layer data resulted in the solid curve in Fig. 9. The experimental results are close to the numerical ray solution. However, the results are consistently slower by a small margin. This was thought to be primarily due to the effects of turbulence. The finite wavelength of the experimental acoustic pulse may also introduce errors between the ray model and the experiment.

Given that the fit between the ray model and the spark experiment is acceptable, the next section looks at how they can be used together to form a measurement system for boundary layer parameters.

V. Boundary layer parameter estimation

The significant quantity for a particular boundary layer is the variation of the mean pulse velocity with acoustic source and microphone spacing, $p(\epsilon)$. This was determined experimentally as given in §IV.B. It was also predicted numerically using the ray method as presented in §IV.A, and denoted $p_e(\epsilon)$. It was seen in the results of Fig. 9 that the two methods resulted in similar functions. Before looking into the identification of TBL parameters, it is useful to introduce a low order model for the mean boundary layer profile.

A. Low order boundary layer model

A boundary layer model for the mean streamwise velocity component as a function of distance from the wall, $U_1 = A(x_2)$ will be defined. This model will have adjustable parameters that allow it to fit a general boundary layer. A simple example used for this paper is Coles¹³ law of the wall and wake. The velocity distribution in the boundary layer is given by Eq. 8 for $x_2 < \delta_t$ and by Eq. 9 and Eq. 10 for $\delta_t < x_2$.¹⁴ Here we will assume that $\delta_t^+ = 10$.

$$\frac{U_1}{u^*} = \frac{u^* x_2}{v} \quad (8)$$

$$\frac{U_0 - U_1}{u^*} = -\frac{1}{\kappa} \ln \frac{x_2}{\delta} + \frac{\Pi}{\kappa} \left[2 - w \left(\frac{x_2}{\delta} \right) \right] \quad (9)$$

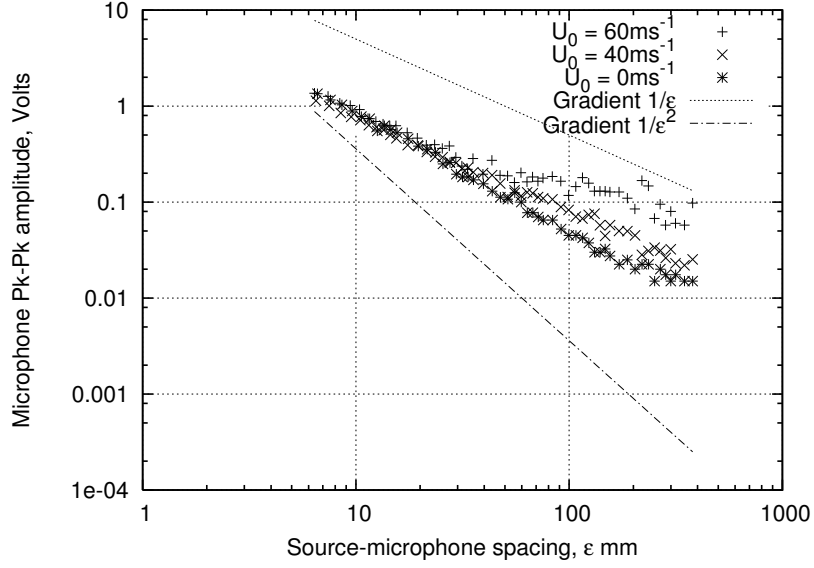


Figure 7. Reduction in pk-pk amplitude of the ultrasonic pulse with distance, with different flow conditions.

$$w\left(\frac{x_2}{\delta}\right) = 1 + \sin\left[\frac{\pi}{2}\left(\frac{2x_2}{\delta} - 1\right)\right] \quad (10)$$

Effectively the boundary layer model given above can be rearranged to give $U_1 = A(x_2, u^*, \delta)$, with other constants held at fixed values. This will be used for boundary layer parameter identification in the following section.

B. Method for estimating boundary layer parameters from experimental results.

Using the ray model an estimation of $p(\epsilon)$, denoted $p_e(\epsilon)$, can be made for a particular boundary layer profile, $A(x_2, u^*, \delta)$. If the ray model is represented by a function R , then we have $p_e(\epsilon) = R(\epsilon, A(u^*, \delta))$.

Given the experimental measurement of $p(\epsilon)$ we would like to determine the values of $[u^*, \delta]$ that cause the ray model to fit the experimental data in the best manner. These values would then constitute a simple measurement of the boundary layer profile. As improvements in the experimental method and modelling method are made, one could increase the number of parameters used in the boundary layer model, resulting in a higher order measurement. However, this two parameter method is suitable for presenting initial results.

Ideally the method for fitting the experimental $p(\epsilon)$ would be achieved by finding an inverse to the ray model, R^{-1} , and solving $A(u^*, \delta) = R^{-1}(p(\epsilon))$. However, since R is a non-linear numerical algorithm, this is clearly not possible. Instead an iterative method was used to minimise an error function, E . A least squares error function between the ray model and experimental results was employed, as given in Eq. 11.

$$E(p(\epsilon), p_e(\epsilon)) = \sum_i [p(\epsilon_i) - p_e(\epsilon_i)]^2 \quad (11)$$

By using the ray and boundary layer model, the error function becomes the result of a numerical procedure as given in Eq. 12.

$$E(u^*, \delta) = \sum_i [p(\epsilon_i) - R(\epsilon_i, A(u^*, \delta))]^2 \quad (12)$$

The error function, Eq. 12, was minimised using the downhill simplex method.¹⁵ Since this is a non-linear minimisation, there is always the possibility of multiple solutions. However, starting the minimisation with different initial conditions resulted in the same solution, giving confidence that the true minimum was found.

Once a solution for $[u^*, \delta]$ was found for a particular experimental measurement of $p(\epsilon)$, the measured boundary layer can be plotted. However, the experimental measurement of $p(\epsilon)$ was only performed over a

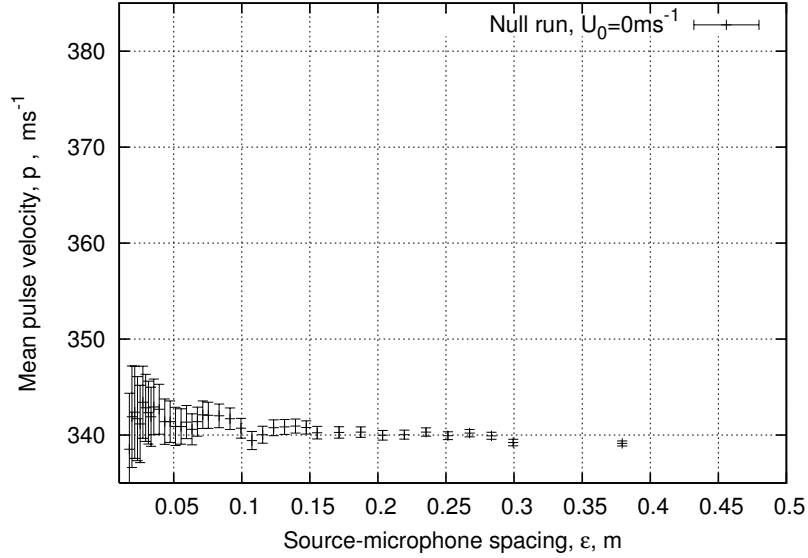


Figure 8. Variation in mean pulse velocity with spacing between source and receiver with no external flow

range of ϵ , bounded by ϵ_{min} and ϵ_{max} . These bounds cause limits in the distance from the wall, x_2 , over which the estimation of boundary layer parameters is valid.

Knowing the estimated $[u^*, \delta]$, the ray path in the $[x_1, x_2]$ plane that corresponds to ϵ_{max} can be computed. This path will have a maximum in its trajectory. This maximum is an upper limit on the range of x_2 that the estimation of the boundary layer parameters is valid.

The case of ϵ_{min} is more complex, but for simplicity it will be treated in the same manner. The ray path in $[x_1, x_2]$ that corresponds to ϵ_{min} is found and its maximum is located. It is assumed that this is the lower bound in x_2 for the measurement of the boundary layer parameters.

A procedure for using experimentally obtained results for $p(\epsilon)$ to estimate boundary layer parameters $[u^*, \delta]$ has been proposed. This procedure employed the ray model and an iterative solution method. In addition the estimated boundary layer parameters have a range of validity given for x_2 .

C. Boundary layer parameter estimation results

The results from the experiments were processed using the method given above. The estimated boundary layer parameters were used to plot the curves shown in Fig. 10. Also shown are the boundary layer profiles measured using a hot-wire anemometer. The agreement is fair over the range of validity of the measurements.

The $40ms^{-1}$ case is also shown plotted using wall units in Fig. 11. This shows that the discrepancy between the hot-wire results and the ultrasonic estimation is larger nearer the wall. This may be expected since the assumptions necessary for the application of ray model are weakest for very near wall measurements. The wavelength of the sound is no longer small when considering near wall measurements. A solution to this would simply be to increase the ultrasound frequency. Another possible source of errors is the effects of turbulent velocities, which were neglected, but become larger relative to the mean near the wall. Lastly, the uncertainty in the experimental results was large for small ϵ (and hence x_2), so experimental uncertainty may also be a factor. Further work in these areas would be interesting.

The numerical method given in this section for the identification of boundary layer parameters was adequate as an example of a data reduction procedure. However, it required moderate computational resources to minimise the error function. For the development of a practical sensor system, it would be advantageous to develop a computationally inexpensive method for data processing. A simple method based upon a look-up table may be more appropriate under these circumstances. The ray model could be used to populate the table.

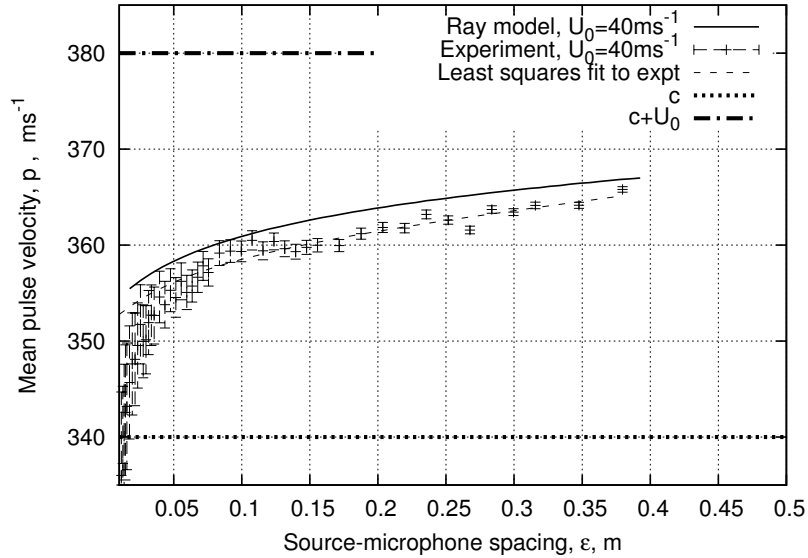


Figure 9. Variation in mean pulse velocity with spacing between source and receiver with presence of boundary layer

VI. Conclusions

The experimental work showed that it is relatively straightforward to perform measurements of the time of flight to different distances downstream. It was apparent from the time series data that the pressure fluctuations due to turbulence in the ultrasonic region were small. The large amplitude pulse pressure typical of a spark was therefore not necessary for the operation of the system. It is suggested that the system could easily be implemented with electrostatic ultrasonic transducers which are more well suited to industrial applications. The scaling of the system has been considered and seems to rest on two factors. These are the boundary layer thickness, and the free-stream Mach number.

For dimensionally thin boundary layers, the central frequency of the pulse (or rise time) has to be high in order that the wavelength of the sound remains small compared to the boundary layer thickness. This is in order that the sound propagates according to geometric acoustics. It can be changed by selecting appropriate transducers.

The sensor system is physically sized based upon the maximum distance downstream from the ultrasound source that a measurement of time of flight is required, ϵ_{max} . The free-stream Mach number affects how large the velocity gradients in the boundary layer are. This affects how much the rays curve in a boundary layer and thus affects the required ϵ_{max} . As an approximate example, measurements from the source of $\epsilon_{max} = 10\delta$ are necessary to resolve the boundary layer up to $x_2 = 0.5\delta$ from the wall at $M = 0.1$. At higher Mach numbers of $M = 0.8$ the furthest distance downstream drops to $\epsilon_{max} = 5\delta$. The exact relationship depends somewhat upon the boundary layer shape in detail. However, as an example, if it was necessary to measure a boundary layer up to $x_2 = 0.5\delta$ that was around $5mm$ thick at $M = 0.8$, the sensor may extend over a length of order $25mm$.

The initial work indicates that it is indeed possible to perform measurements of a mean boundary layer profile using acoustics. The way that acoustic energy is returned to the wall is determined by the mean boundary layer profile. It has been shown that the ray model is appropriate for simply describing the system, although an investigation of the effects of turbulence would be desirable. Using this model it has been possible to perform simple measurements of a boundary layer profile by non-intrusive means. Non-intrusive techniques may prove useful as part of an onboard separation prediction system for aircraft.

Acknowledgments

The author is grateful for the financial support provided by the CAFEDA programme.

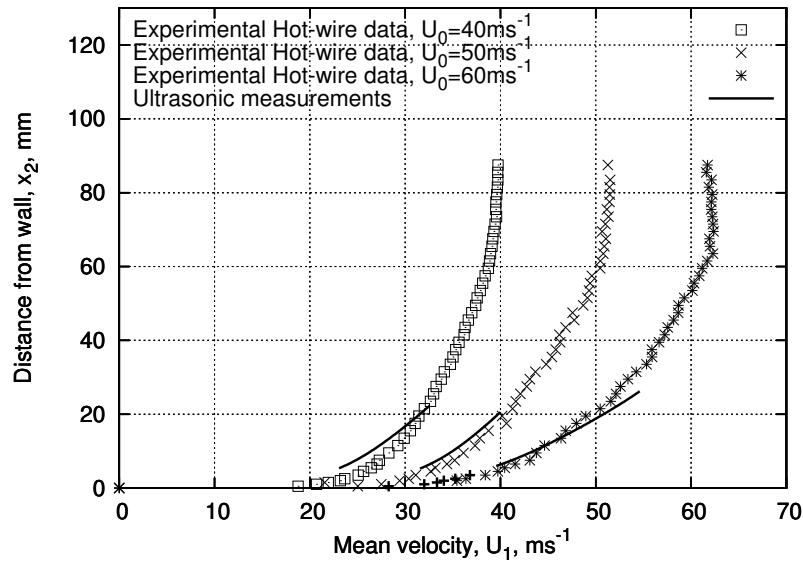


Figure 10. Comparison of ultrasonic prediction and hot-wire measurement of boundary layer profile for three different free-stream velocities

References

- ¹Wetzel T. G., Simpson R. L., and Chesnakas C. J. Measurement of three-dimensional crossflow separation. *AIAA Journal*, 36(4):557–564, April 1998.
- ²Seifert A. and Pack-Melton L. Control and identification of turbulent boundary layer separation. IUTAM symp. on 100 years of boundary layer research, Gottingen, Germany, August 2004.
- ³J.Naughton M.Sheplak. Modern Developments in Shear-Stress Measurement. *PAS*, 38:515–570, 2002.
- ⁴Shen C. and Lemmin U. Ultrasonic scattering in highly turbulent clear water flow. *Ultrasonics*, (35):57–64, 1997.
- ⁵Manneville S., Sandrin L., and Fink M. Investigating a stretched vortex with ultrafast two-dimensional ultrasonic speckle velocimetry. *Physics of fluids*, 13(6):1683–1690, 2001.
- ⁶Schmidt D.W. and Tilmann P.M. Experimental study of sound wave phase fluctuations caused by turbulent wakes. *The journal of the acoustical society of america*, 47(5):1310–1324, 1969.
- ⁷Wilson D.K. and Ostashev V.E. Statistical moments of the sound field propagating in a random refractive medium near an impedance boundary. *The journal of the acoustical society of america*, 109(5):1909–1922, 2001.
- ⁸Ostashev V.E., Wilson D.K., and Liu L. Equations for finite-difference, time-domain simulation of sound propagation in moving inhomogenous media and numerical implementation. *Journal of the acoustical society of america*, 117(2):503–517, 2005.
- ⁹Engelke R. Ray trace acoustics in unsteady inhomogenous flow. *The journal of the acoustical society of america*, 56(4):1291–1292, 1974.
- ¹⁰Pierce A.D. Wave equation for sound in fluids with unsteady inhomogenous flow. *The journal of the acoustical society of america*, 1990.
- ¹¹Cooper J.A., Dewhurst R.J., and Moody S. High-voltage spark discharge source as an ultrasound generator. *IEE Proceedings*, 131(4):275–281, 1984.
- ¹²Wyber R.J. The design of a spark discharge acoustic impulse generator. *IEE Transactions on acoustics, speech and signal processing*, 23(2):157–162, 1975.
- ¹³Coles D. The law of the wake in the turbulent boundary layer. *Journal of fluid mechanics*, 1:191–226, 1956.
- ¹⁴Hinze J.O. *Turbulence*. McGraw-Hill, 1959.
- ¹⁵Press W.H., Teukolsky S.A., Vetterling W.T., and Flannery B.P. *Numerical Recipes in C++*. Cambridge University Press, 2nd edition, 2002.

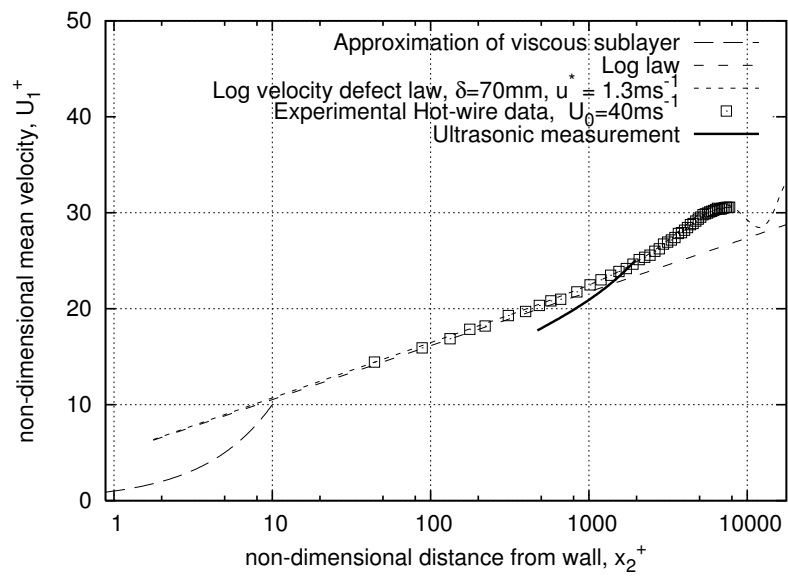


Figure 11. Comparison of ultrasonic prediction and hot-wire measurement of boundary layer profile plotted in wall units